Benchmark Calculation of FHR Fuel Assembly Phase I-C Depletion Exercises

Radomir Ječmenica, Davor Grgić, Paulina Družijanić
University of Zagreb, Faculty of Electrical Engineering and Computing
Unska 3, 10000 Zagreb, Croatia
Radomir.Jecmenica@fer.hr, Davor.Grgic@fer.hr, Paulina.Druzijanic@fer.hr

Bojan Petrović
Georgia Institute of Technology, Nuclear and Radiological Engineering, Atlanta, GA, USA
bojan.petrovic@gatech.edu

ABSTRACT

This paper presents our initial results for the Fluoride-salt High-temperature Reactor (FHR) physics benchmark calculations in Phase I-C, focusing on depletion exercises 5 and 6. In this Phase, the model is extended from the previous OECD benchmarks (Phases I-A and I-B) by transitioning from a pseudo-2D to a full 3D representation of a single FHR fuel assembly featuring TRISO fuel, graphite moderator, and FLiBe coolant. The pseudo-2D geometry is extruded axially, incorporating top and bottom reflectors (FLiBe and graphite), with radial periodic and axial vacuum boundary conditions applied. The benchmark's challenging aspects, including the complex 2D geometry of the plate-type assembly with TRISO fuel, the double heterogeneity spectral calculation, and the use of novel materials (FLiBe coolant and europium as a burnable poison), necessitate the use of Monte Carlo methods. We used the Serpent 2 code (versions 2.1.32 and 2.2.1) with two versions of the ENDF/B library (VI.8 and VII.1). Exercises 5 and 6 subdivide the fuel assembly into 20 axial regions with distinct material temperatures, however the primary distinction between these two exercises is the inclusion of integral burnable absorbers (Eu-151 and Eu-153 oxides) in the latter. The paper presents the results for k_{eff}, recoverable energy per fission, fission density rate, and axial offset in selected burnup points up to the final burnup of 70 GWd/tU. Additionally, we assessed the impact of different cross-section libraries, xenon modeling (transient versus equilibrium), and the depletion step length on the benchmark results.

Keywords: *Serpent 2, Monte Carlo depletion calculation, FHR Benchmark Phase I-C, europium burnable absorber*

1 INTRODUCTION

The Fluoride-salt-cooled High-temperature Reactor (FHR) is an advanced molten salt reactor designed for high operating temperatures at low pressures. It is fuelled with tristructural-isotropic (TRISO) spheres embedded in fuel plates ("planks") of hexagonal fuel elements and cooled with fluoride salt 2LiF-BeF_2 (FLiBe). Due to complex geometry and novelty materials, an evaluation of the applicability of the methodologies and methods used to simulate FHR core physics is needed. Therefore, a benchmark under the auspices of OECD-NEA has been established to assess state of the art modelling and simulation capabilities for FHR reactor type [1]. The benchmark is divided in several phases. In Phase I, a model of a single fuel assembly is analysed. Phase II encompasses a 3D full core model with depletion and Phase III deals with a 3D full core model with feedback and multicycle analysis. Phase I has three subphases: I-A and I-B which cover the pseudo 2D model without and with depletion, respectively [2], and Phase I-C where a 3D model of a single fuel

assembly is analysed [3]. The results of simulations of the pseudo 2D fuel assembly (Phase I-A and Phase I-B) performed by different FHR benchmark participants are published in [4]. In our previous work, we analyzed the first four Phase I-C benchmark exercises [5].

In this paper, we present initial results for Phase I-C depletion exercises 5 and 6. These exercises advance the pseudo-2D model into a comprehensive 3D simulation of an FHR fuel assembly with TRISO fuel, graphite moderator, and FLiBe coolant. The model incorporates an axially extruded geometry with top and bottom reflectors (FLiBe and graphite) and applies radial periodic and axial vacuum boundary conditions. The combination of complex geometry, double heterogeneity, and the use of novel materials (FLiBe coolant and europium as a burnable poison) necessitate application of Monte Carlo methods. We decided to perform calculations using Serpent 2 Monte Carlo code (versions 2.1.32 and 2.2.1 in Windows environment) with the ENDF/B-VI.8 and ENDF/B-VII.1 libraries.

2 METHODOLOGY

2.1 Serpent 2

Serpent [6] is a 3D continuous energy neutron and photon transport code that has been developed at the VTT Technical Research Centre of Finland since 2004. It may be used for a wide range of particle transport applications such as reactor modelling, group constants generation, radiation transport, fusion, etc. The physics model covers neutron, photon and coupled neutron-photon simulations. Cross sections are read from ACE format data libraries. The continuous-energy interaction data is obtained from evaluated nuclear data files without major approximations. Standard tallies in Serpent enable calculating flux, power and reaction rate distributions in geometry cells and materials, as well as regular structures, such as lattices and super-imposed meshes.

2.2 FHR fuel element modelling

FHR is utilizing prismatic fuel assemblies with a hexagonal base divided into three diamond-shaped sections (120 degree rotational symmetry), each containing six fuel planks. The model is shown in Figure 1. The apothem of the fuel hexagon is 22.5 cm and the outer dimension side-to-side is 45.0 cm. FLiBe inter-assembly gap is 1.8 cm, and assembly pitch is 46.8 cm. Each fuel plank is composed of two fuel stripes. Fuel stripes are prismatic regions composed of graphite matrix filled with a cubic lattice of TRISO. In the X–Y plane of each fuel stripe, there are 210×4 TRISO spheres. The TRISO lattice pitch is 0.09266 cm. The cross-section of the fuel element is shown in Figure 2. A TRISO sphere contains 5 layers: fuel kernel, buffer, inner pyrolytic carbon, silicon carbide layer, and outer pyrolytic carbon. Axial distribution of TRISO particles is shown in Figure 3. The control rod is a Y-shape structure made of MHC (Molybdenum-Hafnium Carbide alloy) with no cladding, surrounded by a thin layer of FLiBe. Each control rod wing is 10 cm long and 1 cm thick.

The 3D model of the FHR fuel element was extruded from the pseudo-2D fuel element geometry in axial direction with addition of axial top and bottom reflectors (FLiBe and graphite). Radially, periodic boundary conditions (BC) were applied, and axially vacuum BCs were used (Figure 4).

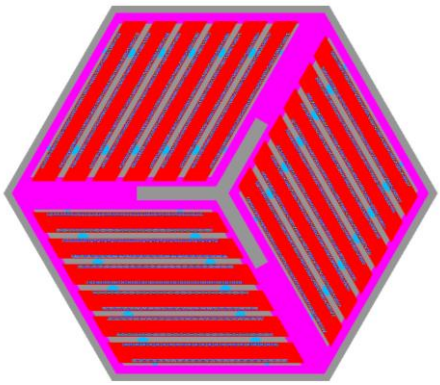

Figure 1: FHR fuel assembly *X-Y* cross section in active fuel part

Figure 2: FHR fuel assembly *X-Y* cross section in active fuel part zoomed to view TRISO spheres

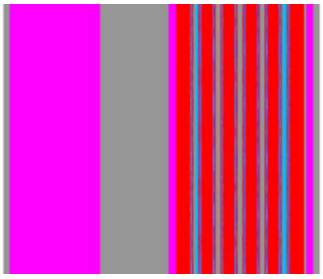

Figure 3: Axial distribution of TRISO spheres

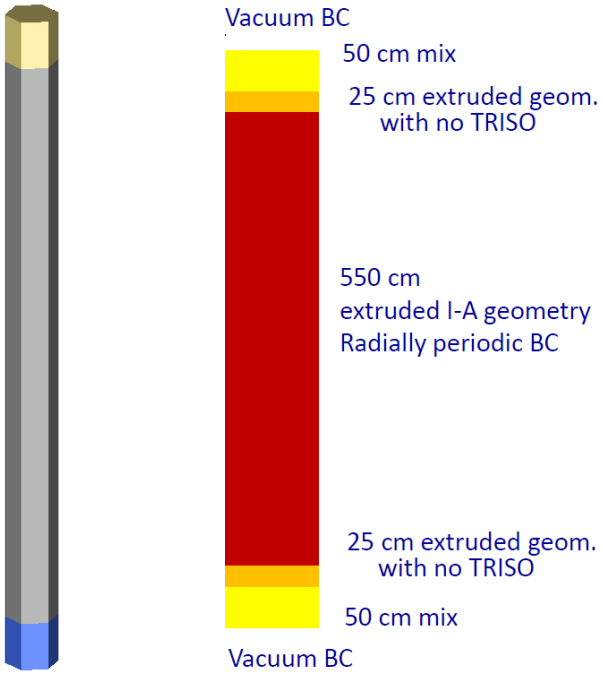

Figure 4: FHR fuel assembly axial division and boundary conditions [3]

2.3 Benchmark exercises

Phase I-C consists of 6 exercises. A summary of all Phase I-C exercises is given in Table 1. Exercises 1 - 4 were analysed in our previous work [5]. The first Phase I-C depletion exercise is Exercise 4. It assumes an axially symmetric core with uniform temperature and depletion is performed for a single axial fuel zone. Exercises 5 and 6 use a fuel assembly model consisting of 20 axial regions, bottom and top axial reflectors, bottom and top extruded geometry (the same as fuel region but without TRISO spheres), and 16 equidistant regions within active fuel. Axially, each region contains 371 TRISO spheres. These regions have different but fixed material temperatures (fuel kernel, graphite, and FliBe). The difference between Exercises 5 and 6 is in the presence of integral burnable absorbers (BA) in the latter case.

Burnable absorbers (in the form of Eu_2O_3) are contained in spheres with a radius of 0.035 cm. The axial distance between the centres of these spheres is 0.09266 cm, which means that each axial

region contains 371 BA spheres. Axially, the centres of the TRISO spheres and the BA spheres coincide. In each of the 371 subregions within every plank, there are five BA spheres spaced 4 cm apart. Radially, the central BA sphere in each plank is positioned at half the width of the cooling channel.

The paper presents the results for k_{eff}, recoverable energy per fission, fission density rate, and axial offset in selected burnup points up to the final burnup of 70 GWd/tU. In addition to the influence of used cross-section libraries, we studied the influence of assumption on transient or equilibrium Xe during depletion and the length of integration step on the calculated results.

Table 1: Description of Phase I-C exercises

Exercises	Description
1	Axially symmetric core Uniform Axial Temperature, fuel kernel 1110 K, everything else 948 K
2	Reported vs actual convergence, the same as Exercise 1, but more spatial results requested
3	Control Rod insertion
4	Depletion as single region
5	Modified Exercise 4 with axial temperature distribution and fission density rate and depletion in 16 fuel zones
6	Modified Exercise 5 with discrete Eu poison present

The power density during depletion calculations was assumed constant at 200 W/gU. To satisfy the condition $\sigma_{k\text{-eff}} < 15 \cdot 10^{-5}$, 500 active generations with 50,000 neutrons per generation were used. A single burnup step under these conditions (Exercise 6) takes approximately three hours using ENDF/B-VII.1, and the program requires unreasonably long time (and large amount of memory) just to initiate the depletion calculation. For this reason, the calculations were performed first using the ENDF/B-VI.8 library. Planned comparison with SCALE burnup calculation results was cancelled because we used SCALE Windows version which does not have parallel capability and estimated running time was too long.

3 RESULTS

3.1 Exercise 5 results

The results of the Exercise 5 are k_{eff}, recoverable energy per fission, fission density rate, and axial offset calculated at selected burnup (BU) points up to the final burnup of 70 GWd/tU.

To illustrate the influence of the libraries used in the calculations, Figure 5 presents k_{eff} values during depletion for two different libraries, ENDF/B-VII.1 and ENDF/B-VI.8, while Figure 6 shows corresponding fission density rates axial distributions for Middle Of Cycle (MOC) and End Of Cycle (EOC). Figure 5 indicates that newer library gives lower k_{eff} values. The difference in effective multiplication factors is generally between 300 and 350 pcm, dropping below 150 pcm only at the initial burnup points. The choice of cross-section library has a non-negligible impact on the effective multiplication factor. Additionally, the cross-section library somehow affects the axial power distribution – not only in terms of Fission Density Rate (FDR) magnitudes but also in the sign of the axial offset. It is likely that at least AO differences are not just due to different libraries, but are due to a combination of library data, statistical uncertainty and the presence of Xe oscillations. A similar trend is observed in the axial power distribution at the end and at the middle of the cycle.

In Figure 7 axial offset as a function of burnup for equilibrium Xe and transient Xe calculation assumptions (22 BU points) is presented. As expected, the equilibrium xenon option results in lower absolute values of the axial offset during depletion.

Figure 8 presents the end-of-cycle axial distribution of U-235, Pu-239, and Xe-135 concentrations for different cross-section libraries and xenon calculation options. The U-235 concentration EOC axial distribution remains unaffected by the choice of cross-section library or xenon treatment during burnup (transient vs. equilibrium xenon). The impact of the cross-section library on Pu-239 concentration is relatively weak, whereas its effect on Xe-135 concentration is somewhat more pronounced. Xe calculation option has some influence on Xe distribution only.

Figure 9 presents the fission density rate for different numbers of burnup points (NEW: 22 points and FINE: 37 points) at 45, 50, and 65 GWd/tU. According to the Benchmark specifications, the obtained results should be provided at predefined burnup points. Depletion calculations were initially performed in 22 steps; however, unexpectedly early deviations in axial power distribution values were observed toward the end of the cycle, including changes in the sign of the axial offset. To address this, a depletion calculation was conducted using 37 burnup points (labelled as "FINE" in Figure 9), but the issue persisted, albeit to a lesser extent. The use of a newer cross-section library (ENDF/B-VII.1) might help resolve this issue, but equilibrium Xe calculation has inherent dependency on size of burnup step.

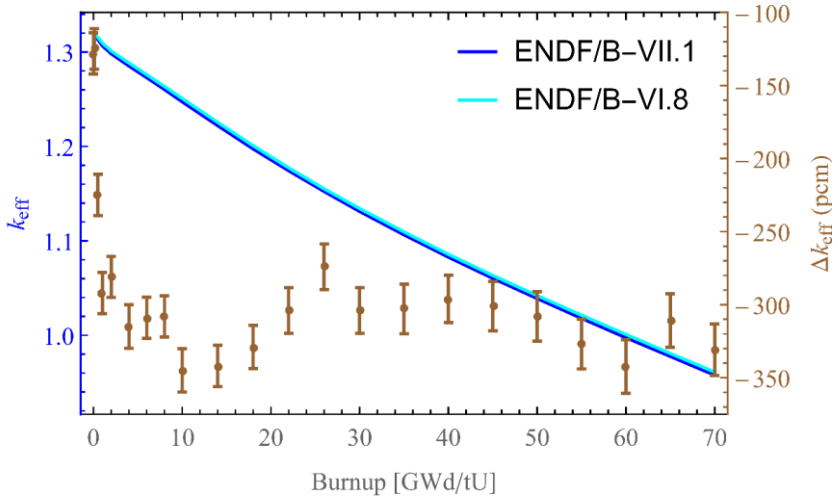

Figure 5: k_{eff} during depletion for two cross section libraries

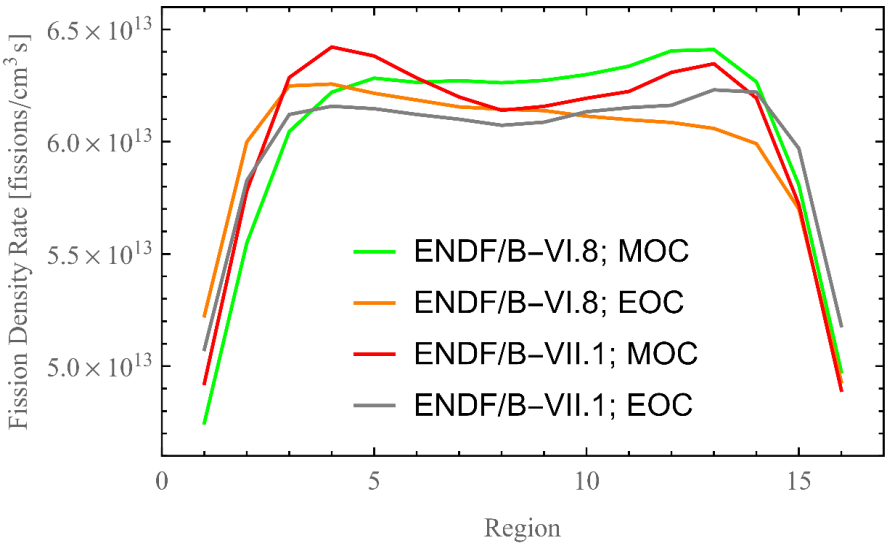

Figure 6: Effect of the cross-section library on MOC and EOC axial distributions.

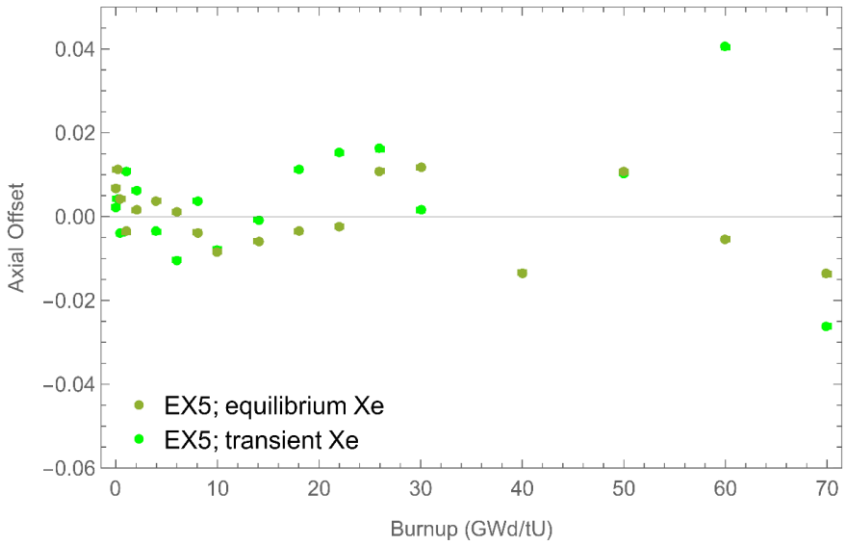

Figure 7: Axial offset vs. burnup for equilibrium Xe and transient Xe calculation assumptions (22 BU points)

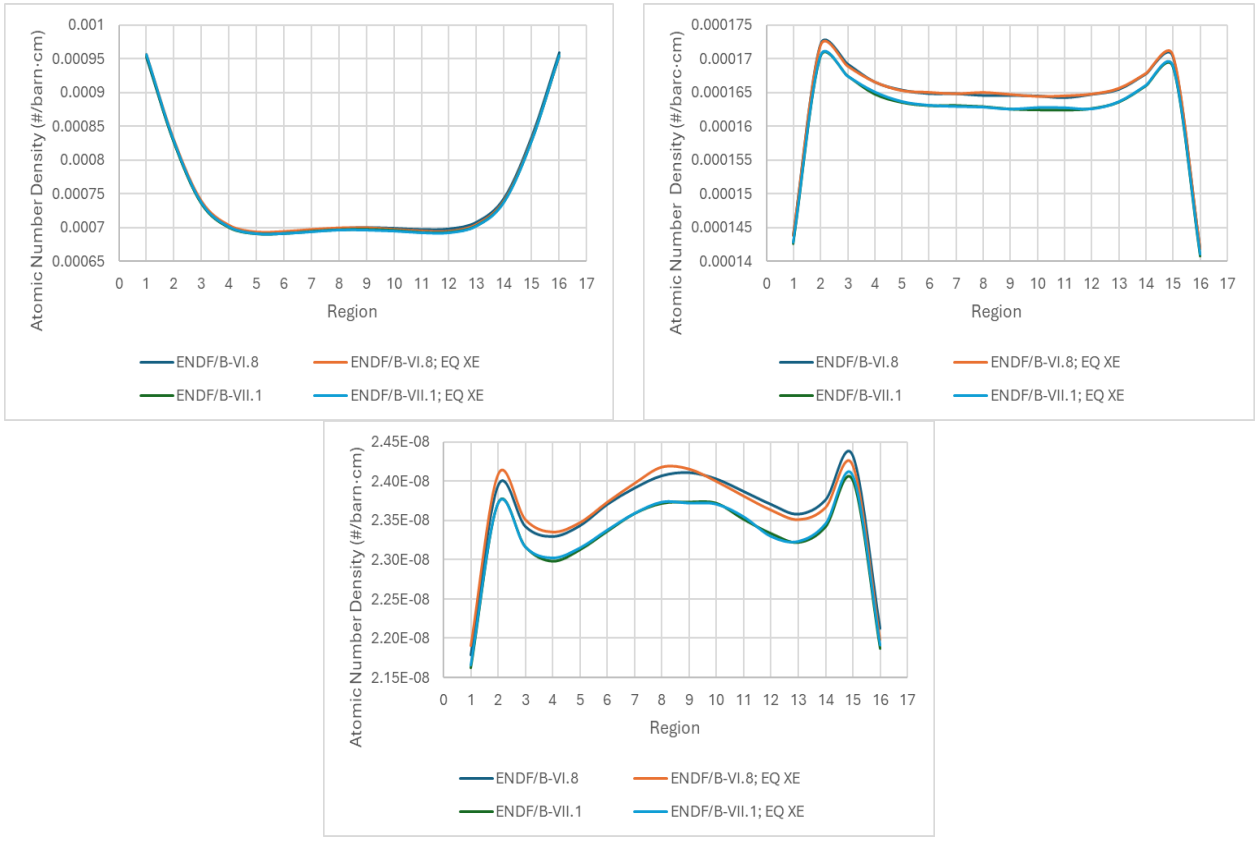

Figure 8: EOC axial distribution of U-235, Pu-239 and Xe-135 concentration for different libraries and Xe calculation options

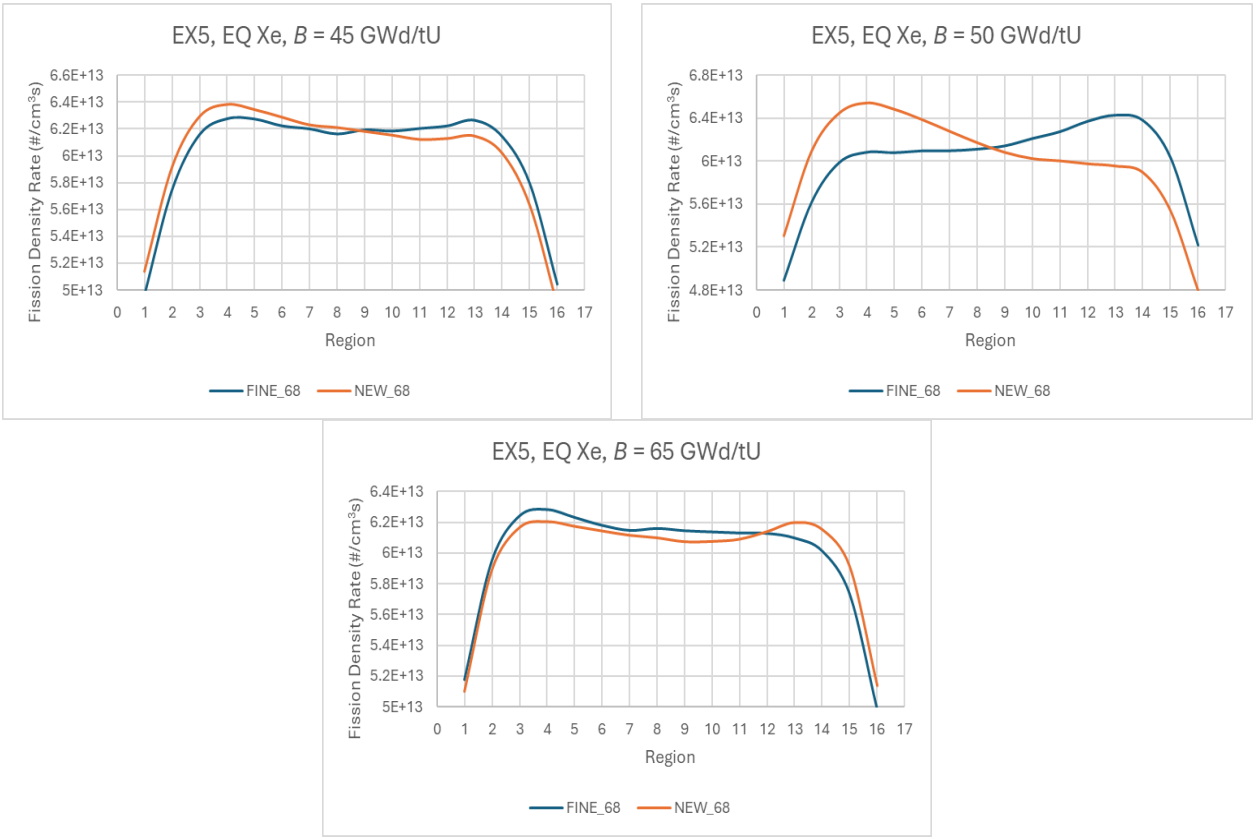

Figure 9: Fission density rate for different number of depletion BU points (NEW 22 BU points, FINE 37 BU points) for 45, 50 and 65 GWd/tU

3.2 Exercise 6 results

The results of the Exercise 6 are k_{eff}, recoverable energy per fission, fission density rate, and axial offset calculated in selected burnup points up to the final burnup of 70 GWd/tU.

Figure 10 shows k_{eff} values for two cross-section libraries. At the beginning of depletion, the obtained k_{eff} values differ significantly – by up to 800 pcm. As the Eu-151 concentration decreases due to depletion, Δk_{eff} drops below 100 pcm. However, by the end of the cycle, it reaches approximately 400 pcm. Figure 10 clearly illustrates the significant impact of the cross-section library on $k_{eff}(B)$, the same as before the use of ENDF/B-VII.1 library results in lower k_{eff} values.

Figure 11 presents a comparison of the axial burnup distributions for Exercise 5 and Exercise 6 at MOC (30 GWd/tU) and EOC (70 GWd/tU). The impact of the cross-section library on the axial power distribution at MOC and EOC is not significant. In all considered cases, the obtained curves are smooth, with no obvious differences between them. Burnups obtained in exercise with integral burnup absorbers are typically higher in central part of the core.

Figure 12 shows the fission density rate axial distributions for BOC/MOC and EOC using two cross section libraries. Besides its magnitude, the differences are also evident in the shape of the FDR(z) curve, particularly in the sign of the axial offset. This effect is especially pronounced at the end of the cycle. As before, it is difficult to determine whether these differences are caused solely by library selection or by related statistical uncertainty and the presence of Xe instability.

Figure 13 presents the axial offset as a function of burnup for equilibrium Xe and transient Xe calculation assumptions (22 BU points). Based on Figure 13, it can be concluded that the equilibrium xenon option predominantly results in lower absolute values of the axial offset.

The EOC axial distribution of Eu-151 and Eu-153 concentrations for depletion with equilibrium and transient Xe is shown in Figure 14. Based on Figure 14, it can be concluded that different xenon treatments during depletion (transient vs. equilibrium Xe) have some impact only on the final concentration of the Eu-151 isotope, but not on the Eu-153 isotope.

Due to the burnable absorber presence and related spectral effects, the recoverable energy per fission values are consistently higher for Exercise 6 than for Exercise 5, as shown in Figure 15 for ENDF/B-VI.8 library and equilibrium Xe assumption used in calculation.

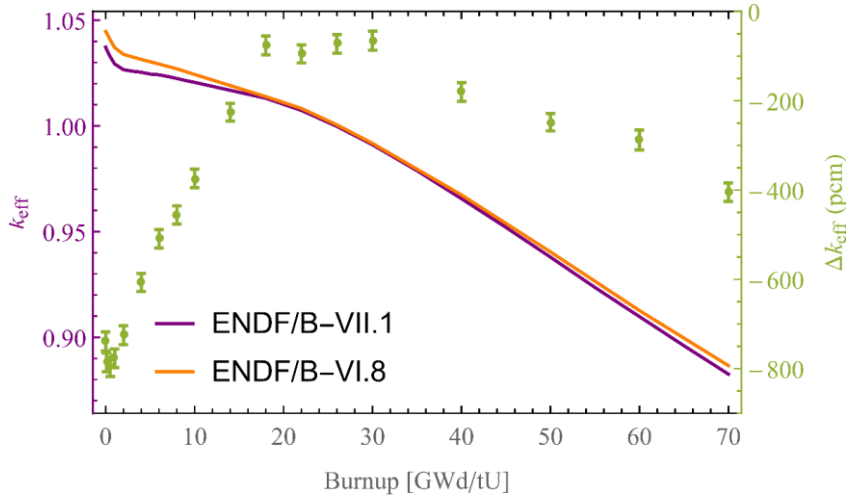

Figure 10: k_{eff} during depletion for two cross section libraries

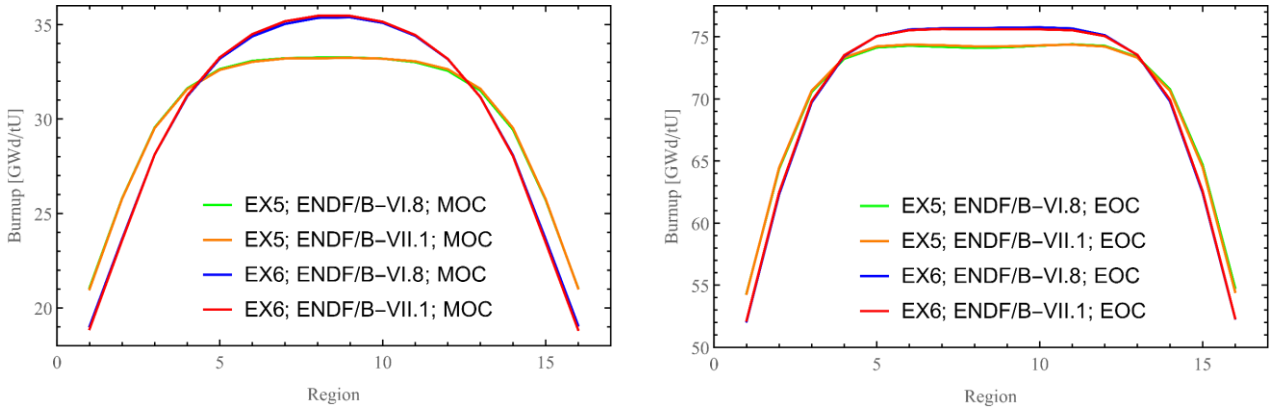

Figure 11: Axial burnup distribution for MOC (30 GWd/tU) and EOC (70 GWd/tU), Exercise 5 and 6 (Eu as BA)

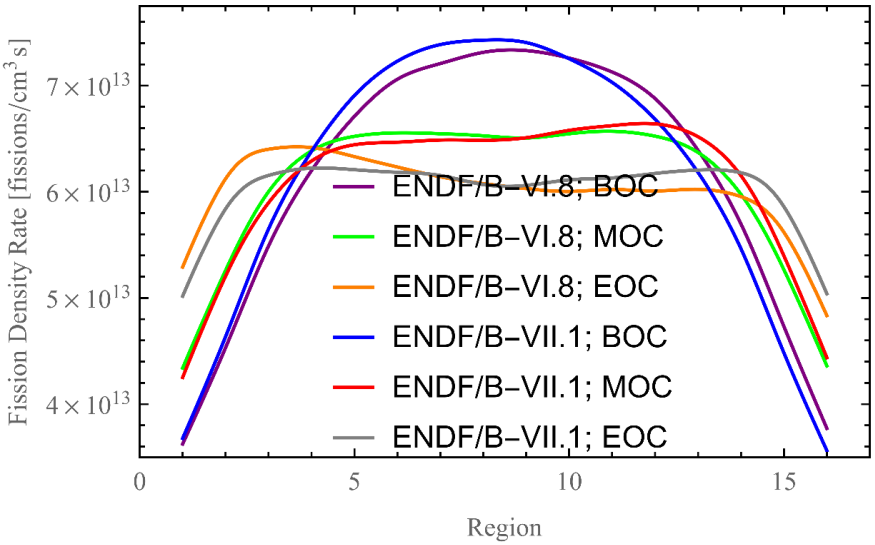

Figure 12: The influence of used library on BOC, MOC and EOC axial distributions

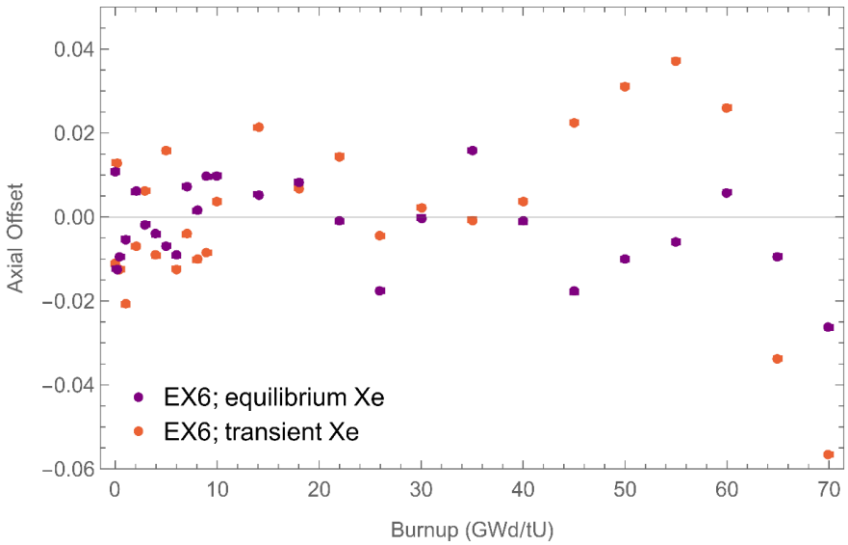

Figure 13: Axial offset vs. burnup for equilibrium Xe and transient Xe calculation assumptions

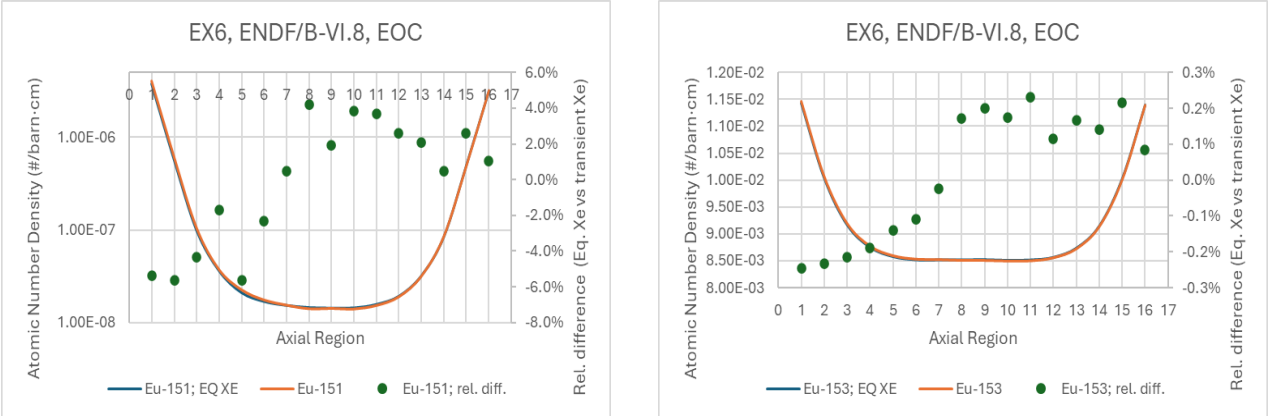

Figure 14: EOC Eu-151 and Eu-153 concentration axial distribution for depletion with equilibrium and transient Xe

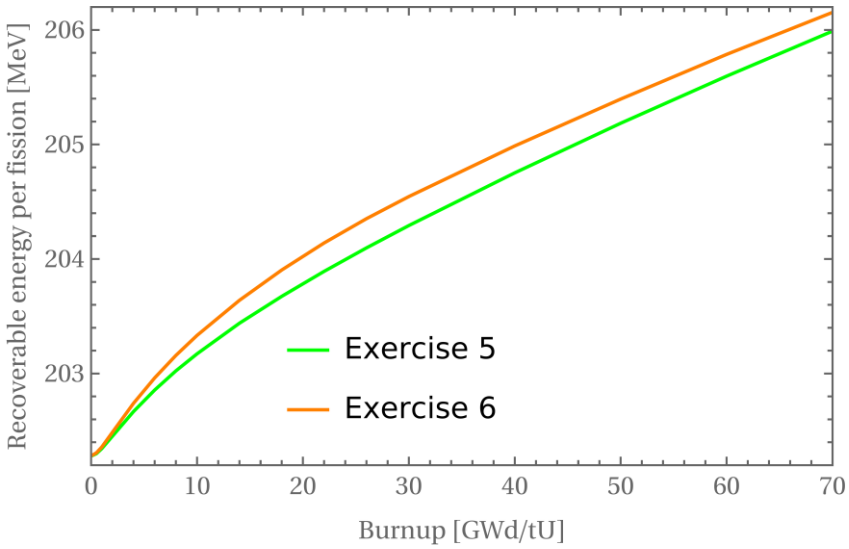

Figure 15 Recoverable energy per fission as function of burnup, ENDF/B-VI.8, eq. Xe

4 CONCLUSION

The initial results for Fluoride-salt High-temperature Reactor (FHR) reactor physics benchmark calculations, Phase I-C, depletion exercises 5, and 6 were presented. In addition to assessing the impact of the cross-section libraries used, we studied the influence of assumption on transient or equilibrium Xe treatment during depletion calculation and the length of depletion step on the calculated results. As expected, the choice of cross-section library significantly affects both k_{eff} and recoverable energy per fission. Some impacts are observed in the axial distributions of power and isotopic concentrations. Due to the nature of assumptions made during depletion calculation, both length of burnup step and method used in the calculation of Xe concentration (equilibrium or full transient) have impact on the EOC axial power distributions. Therefore, more detailed guidelines (such as the number and the size of burnup steps or the assumption on Xe treatment) and more clear simulation requirements should be provided to be able to use each calculation tool specific capabilities and to simplify comparison of results between participants.

The Serpent 2 code has proven to be a good choice for this demanding modeling problem, considering aspects such as input preparation, code capabilities, and execution time. The selection of the cross section library is influencing both the obtained results and required computation time. Notably, a significant increase in calculation time and memory usage was observed during the preparatory phase of the Serpent 2 depletion calculations when switching from the ENDF/B-VI.8 to the ENDF/B-VII.1 library. Consequently, it is reasonable to perform all initial and sensitivity calculations using ENDF/B-VI.8 library and use ENDF/B-VII.1 library for the final calculations only.

REFERENCES

[1] K. M. Ramey, B. Petrovic, “Monte Carlo modeling and simulations of AHTR fuel assembly to support V&V of FHR core physics methods”, Annals of Nuclear Energy, 118 2018, pp. 272-282

[2] Benchmark Specifications for the Fluoride-salt High-temperature Reactor (FHR) Reactor Physics Calculations, NEA/NSC/R(2020)5, March 2021

[3] B. Petrovic, J. Faulkner, “Benchmark Specifications for the Fluoride-salt High-temperature Reactor (FHR) Reactor Physics Calculations Phase I-C: Fuel Element 3D Benchmark,” in preparation, NEA Nuclear Science, OECD Publishing, Paris, France.

[4] K. M. Ramey et al., “Impact of molybdenum cross sections on FHR analysis”, Nuclear Engineering and Technology, 54, 2022, pp. 817-825

[5] R. Ječemenica, D. Grgić, B. Petrović, P. Dučkić, Usage of Monte Carlo Code Serpent2 for Calculation of FHR Fuel Assembly, Proceeding of the International Conference Nuclear Energy for New Europe, 11-14 September 2023, Portorož, Slovenia

[6] J. Leppänen et al., "The Serpent Monte Carlo code: Status, development and applications in 2013."Ann. Nucl. Energy, 82, 2015, pp. 142-150